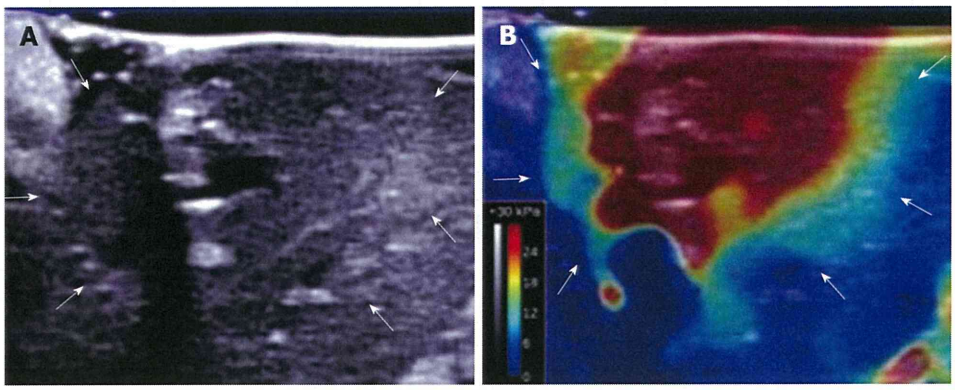

Figure 2 B-mode ultrasound image and shear-wave elastography image of a thermal lesion. A: B-mode ultrasound image of the liver obtained 15 min after ablation shows a poorly defined hypoechoic lesion with a hyperechoic rim (arrows); B: Corresponding shear-wave elastography image of the liver clearly delineates the ablated area (arrows).

performed by slow-tilt movement of the mechanical sector transducer with a sweep angle of 30°. After the US examination was completed, the acquired 3D volume data were rendered and saved in the US system console as a multislice display (interslice distance: 1.10 mm) for off-line analysis, including ablation volume measurement.

Tissue collection and histological analysis

The animals were sacrificed after completion of the US examinations, and the livers were harvested. To permit radiologic-pathologic correlation, US was used to guide cutting of the livers in the proper sectional planes along the course of the ablation electrode. After formalin fixation, the livers were cut by total segmentation and digitized photographs of the cut surfaces were obtained. The photographs were used to estimate the volume of the 10 thermal lesions. For histopathological examination, the liver specimens were embedded in paraffin and cut with a microtome to obtain 3-μm sections. The sections were then stained with hematoxylin and eosin (H-E) or an anti-heat shock protein 70 (Hsp70) antibody (sc-24; Santa Cruz Biotechnology, Dallas, TX, United States) according to the manufacturer's instructions.

SWE and pathological volume measurements

The estimated volumes of the 10 thermal lesions were used to assess the correlation between SWE findings and the digitized photographs of the gross pathological specimens. The estimated volume of each lesion in the gross pathological specimens was calculated by summing the values obtained by multiplying the area of the thermal lesion in each section by the section thickness (3 mm). For SWE, the volume of each lesion was automatically calculated by summing the values obtained by multiplying the area of the thermal lesion in each 2D SWE image by the scan plane interval (1.10 mm). All RF ablation areas in the SWE images as well as in the digitized photographs of the gross pathological sections were manually delineated based on the consensus of two observers.

Statistical analysis

All data are presented as mean ± SD. The differences in the detectability of RF ablation lesion boundaries between SWE and B-mode US imaging were evaluated using the McNemar test. A value of $P < 0.05$ was considered to indicate a statistically significant difference between the groups. The accuracy of the various volume measurements was compared with the reference standard (pathological findings) using multiple linear regression analysis. All statistical analyses were performed with the SPSS 11.0 computer software package (SPSS, Tokyo, Japan).

RESULTS

US findings after RF ablation

For each SWE image, the tissue stiffness of each pixel was displayed as a semitransparent color overlay with a range from dark blue, indicating the lowest stiffness (just over 0 kPa), to red, indicating the highest stiffness (set at 30 kPa). SWE images after RF ablation clearly delineated the ablated area, which is seen as a red area surrounded by a yellow-green area (Figure 2B). The surrounding yellow-green area, which exhibited sinusoidal dilatation accompanied by congestion in the H-E sections, was observed in all RF-ablated lesions. On the other hand, B-mode US after RF ablation showed a poorly defined hypoechoic lesion with a hyperechoic rim (Figure 2A).

All RF ablation areas in the maximal plane of the SWE images as well as in the B-mode images were manually delineated based on the consensus of two observers. Table 1 shows a comparison of the detectability of RF ablation lesion boundaries between SWE and B-mode images. The boundaries of all 10 thermal lesions (100%) were completely delineated by SWE, while only 3 lesions (30%) could be completely delineated in the B-mode images. The other 7 lesions (70%) could only be partially delineated in the B-mode images. The difference in lesion detectability between the two techniques was found to be statistically significant ($P = 0.001$).

In each shear-wave image of the RF ablation area, circular regions of interest (ROIs) measuring 3 mm in diameter were specified in the central red zone, the surrounding yellow-green zone, and the non-ablated zone (3 ROIs in each zone). The mean tissue stiffness values of

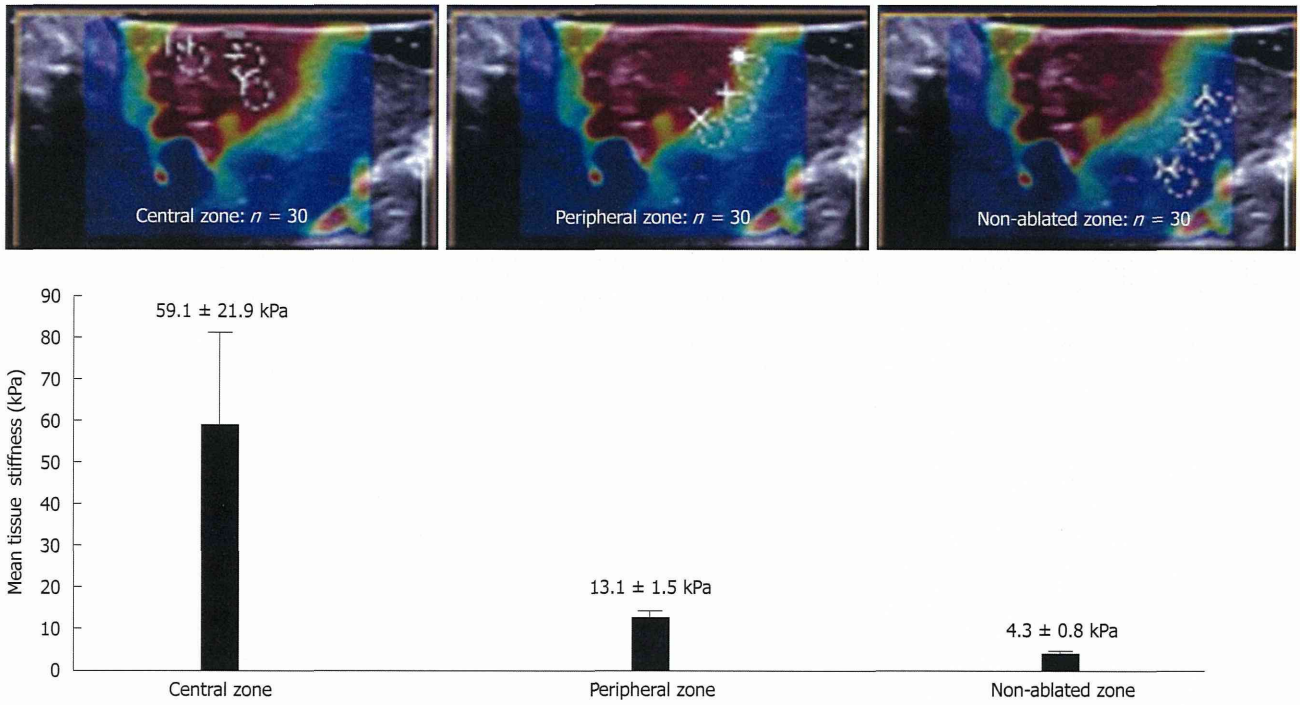

Figure 3 Liver tissue stiffness values of the thermal lesions. Mean tissue stiffness of the central zone, peripheral zone, and non-ablated zone of the livers after radiofrequency ablation. The images at the top show examples of how the regions of interest in each zone were selected.

Table 1 Boundary detection of thermal lesions using B-mode ultrasound and shear wave elastography *n* (%)

Boundary detection	B-mode (*n* = 10)	SWE (*n* = 10)
Complete	3 (30)	10 (100)
Partial	7 (70)	0 (0)

All radiofrequency (RF) ablation lesions visualized by shear-wave elastography (SWE) and B-mode ultrasound were manually delineated based on the consensus of two observers. Complete: Complete delineation of RF ablation lesion boundaries; Partial: Partial delineation of RF ablation lesion boundaries.

the central zone, the peripheral zone, and the non-ablated zone were 59.1 ± 21.9 kPa, 13.1 ± 1.5 kPa, and 4.3 ± 0.8 kPa, respectively (Figure 3).

Pathological findings after RF ablation

In the gross pathological specimens, the regions affected by RF ablation could be easily distinguished from unaffected liver tissue based on their colors after formalin fixation. The heat-coagulated lesions appeared light tan to gray and were consistently observed to have a dark brown rim of vascular congestion (Figure 4A). These gross pathological changes correlated well with the histopathological findings. Specifically, the rim of vascular congestion identified by gross pathological examination was histopathologically characterized by sinusoidal dilatation, hemostasis, hemorrhage, and overexpression of Hsp70 in hepatocytes, which accurately discriminated the heat-coagulated lesions from the unaffected normal liver tissue in all samples (n = 10) (Figure 4B, C, and D). A high correlation was observed between the volumes depicted by SWE and those estimated by gross pathological examination (r^2 = 0.9305) (Figure 5).

DISCUSSION

The results of the present study using normal rat livers demonstrate that the depiction of thermal lesions by SWE agrees closely with the findings of gross pathological examination. SWE is therefore expected to be useful for clearly visualizing thermal lesions and obtaining quantitative volume estimates. Comparison between the ablation volumes depicted by SWE and those estimated by gross pathological examination showed a high correlation (r^2 = 0.9305). These findings suggest that 3D SWE may prove to be an accurate and convenient tool for monitoring early treatment effects after RF ablation.

At present, contrast-enhanced US[7], contrast-enhanced computed tomography[8], and magnetic resonance imaging[9] are considered to be suitable methods for depicting ablation zones by demonstrating the absence of contrast enhancement when performed at an appropriate time after the ablation procedure. However, in order to perform virtual real-time monitoring of an ablation procedure, repeated contrast injection is required because there is only a short time frame in which the lesion is detectable before equilibrium is reached. These modalities are therefore unsuitable for real-time monitoring during RF ablation procedures, making it difficult to precisely evaluate the ablation zone at the time of treatment. Moreover, an enhanced rim is usually observed in contrast images, which may be difficult to differentiate from an enhanced rim indicating an area of residual untreated

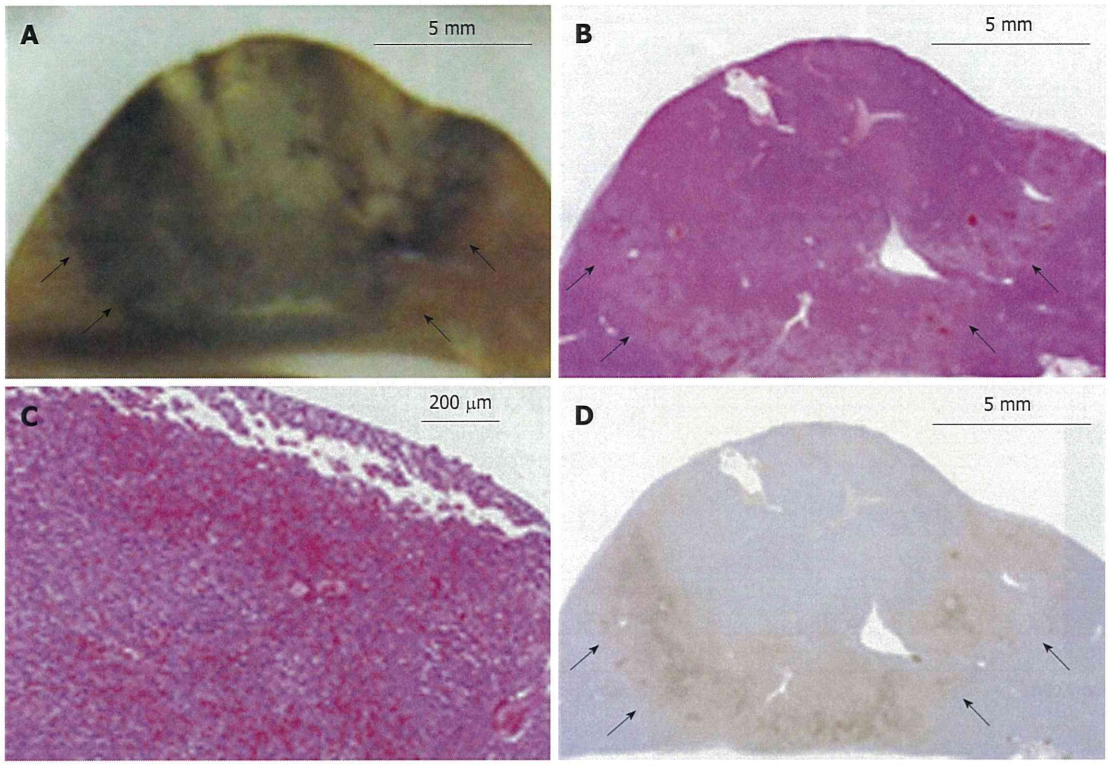

Figure 4 Histopathological findings of a thermal lesion. A: Gross pathological examination of a radiofrequency (RF)-ablated liver shows a core area of white coagulation and a surrounding dark rim of hemorrhagic tissue (arrows). Scale bar: 5 mm; B, C: H-E staining of an RF-ablated liver shows a hemorrhagic rim surrounding the ablated area (arrows), with sinusoidal dilatation and congestion associated with cellular dissociation. Scale bar in (B): 5 mm, and in (C): 200 μm; D: Hsp70 staining of the hemorrhagic rim in (B) shows a clearly demarcated band of Hsp70 expression (arrows), which is suggestive of the presence of thermally damaged cells within the rim. Scale bar: 5 mm.

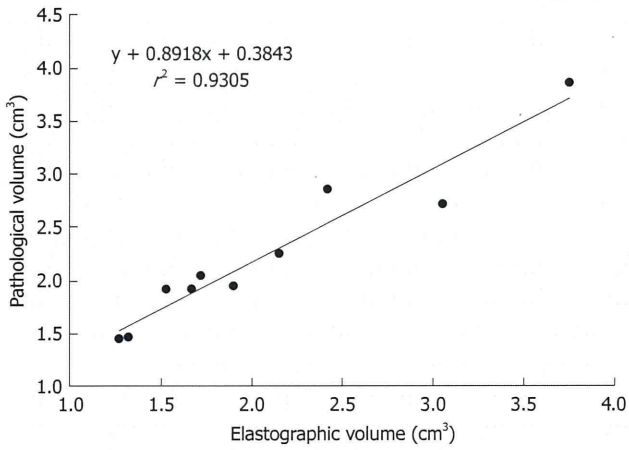

Figure 5 Correlation between shear-wave elastography and gross pathological findings. The correlation between the volume of liver ablation depicted by 3D shear-wave elastography and that estimated by gross pathological examination was 0.9305, which is highly significant.

tumor. For these reasons, SWE may prove to be a more useful method for real-time monitoring in RF ablation procedures.

The H-E staining technique relies on visual examination of the cell membranes and intracellular structures to assess cell viability. Morimoto *et al*[8] have shown that H-E staining provides inconsistent results regarding the extent, or completeness, of tissue necrosis when performed less than 24 h after the application of the necrosis-inducing agent. Therefore, histochemical staining methods, such as those employing lactate dehydrogenase, malate dehydrogenase, and nicotinamide adenine dinucleotide phosphate (NADPH) diaphorase, are thought to be superior to H-E staining for identifying irreversible cellular damage after RF ablation. Accordingly, Morimoto *et al*[8] also evaluated heat-coagulated lesions after RF ablation by analyzing cell viability within the lesions using histochemical staining (lactate dehydrogenase, malate dehydrogenase, and NADPH diaphorase). They found that the regions of heat coagulation (*i.e.*, the central areas of the ablated lesions) were not stained in any of the samples, suggesting 100% cellular destruction within the lesion. Moreover, the surrounding hemorrhagic rim (*i.e.*, the peripheral part of the ablated lesion) was also not histochemically stained in any of the samples, suggesting the disappearance of viable cells from the rim as well. Based on these findings, we also assumed that viable cells were absent from the surrounding narrow rim of vascular congestion observed in our study. Interestingly, a thick rim of Hsp70 staining, which is a marker of thermal damage, was noted in the area peripheral to the ablation zone, which corresponded to the congestive rim. Hsp70 may therefore be a useful biomarker for assessing cell viability after thermal damage[10].

In our study, the mean tissue stiffness of the hemorrhagic rim was 13.1 ± 1.5 kPa, and our findings suggest that this may be an appropriate threshold value for deter-

mining irreversible cellular destruction. This value may also be of clinical significance because an incompletely ablated area should be softer (*i.e.*, less than 13.1 kPa) and show higher contrast than surrounding completely ablated areas, which may provide useful information for guiding a second round of RF ablation to treat the incompletely ablated area.

It should be noted that our study suffers from a number of limitations. First, the study was performed in normal rat livers. Similar studies should be performed in a liver tumor model or in cirrhotic livers to increase the clinical relevance of the findings. Second, cell viability was assessed only by H-E staining and by immunohistochemical analysis of Hsp70. Assessment of cell viability using more reliable methods should be performed in future studies. Third, at present, contrast-enhanced computed tomography and magnetic resonance imaging are considered to be suitable methods for depicting ablation zones by demonstrating the absence of contrast enhancement, but we did not compare SWE against these modalities in our study. Nevertheless, SWE has been shown to be an effective, safe, and cost-efficient tool for evaluating tumor treatment in the interventional suite immediately after ablation.

In conclusion, 3D SWE is a reliable noninvasive technique that may allow the real-time assessment of treatment efficacy immediately after RF ablation procedures. The threshold value for determining remaining cell viability was found to be 13.1 ± 1.5 kPa.

COMMENTS

Background

The ability to assess the completeness of radiofrequency (RF) ablation during or immediately after the procedure would be of great clinical value. If three-dimensional (3D) shear-wave elastography (SWE) is found to be superior for precise assessment of the ablation area, it would be a better method for assessing the completeness of RF ablation because the administration of contrast agent is not required and both 3D assessment and real-time observation are possible.

Research frontiers

To the best of our knowledge, no other investigators have reported on the usefulness of 3D SWE for evaluation of the ablated area after RF ablation procedures.

Innovations and breakthroughs

3D SWE is a reliable noninvasive technique that may allow the real-time assessment of treatment efficacy immediately after RF ablation procedures. It is superior to B-mode ultrasound (US) in delineating ablated areas in the liver.

Applications

By providing a clearer understanding of how closely the boundaries of thermal lesions visualized by 3D SWE correspond to the actual boundaries of tissue ablation determined by histological examination, this study may lead to improved local ablation therapy in patients with hepatic malignancies.

Terminology

Among the various techniques employed in US elastography, SWE is a highly reproducible method that allows measurement of the propagation speed of shear waves within tissues for the local quantification of tissue stiffness in kilopascals or meters per second.

Peer review

The manuscript titled "Radiologic-pathologic correlation of three-dimensional shear-wave elastographic findings after radiofrequency ablation" regards the evaluation of RF ablation with the SWE compared to simple B mode, which is a generally well-written paper focused on an important topic.

REFERENCES

1 **Livraghi T**, Goldberg SN, Lazzaroni S, Meloni F, Solbiati L, Gazelle GS. Small hepatocellular carcinoma: treatment with radio-frequency ablation versus ethanol injection. *Radiology* 1999; **210**: 655-661 [PMID: 10207464]

2 **Shiina S**, Tateishi R, Arano T, Uchino K, Enooku K, Nakagawa H, Asaoka Y, Sato T, Masuzaki R, Kondo Y, Goto T, Yoshida H, Omata M, Koike K. Radiofrequency ablation for hepatocellular carcinoma: 10-year outcome and prognostic factors. *Am J Gastroenterol* 2012; **107**: 569-577; quiz 578 [PMID: 22158026 DOI: 10.1038/ajg.2011.425]

3 **Huang J**, Yan L, Cheng Z, Wu H, Du L, Wang J, Xu Y, Zeng Y. A randomized trial comparing radiofrequency ablation and surgical resection for HCC conforming to the Milan criteria. *Ann Surg* 2010; **252**: 903-912 [PMID: 21107100 DOI: 10.1097/SLA.0b013e3181efc656]

4 **Ferraioli G**, Tinelli C, Dal Bello B, Zicchetti M, Filice G, Filice C. Accuracy of real-time shear wave elastography for assessing liver fibrosis in chronic hepatitis C: a pilot study. *Hepatology* 2012; **56**: 2125-2133 [PMID: 22767302 DOI: 10.1002/hep.25936]

5 **Youk JH**, Gweon HM, Son EJ, Chung J, Kim JA, Kim EK. Three-dimensional shear-wave elastography for differentiating benign and malignant breast lesions: comparison with two-dimensional shear-wave elastography. *Eur Radiol* 2013; **23**: 1519-1527 [PMID: 23212276 DOI: 10.1007/s00330-012-2736-3]

6 **Kolokythas O**, Gauthier T, Fernandez AT, Xie H, Timm BA, Cuevas C, Dighe MK, Mitsumori LM, Bruce MF, Herzka DA, Goswami GK, Andrews RT, Oas KM, Dubinsky TJ, Warren BH. Ultrasound-based elastography: a novel approach to assess radio frequency ablation of liver masses performed with expandable ablation probes: a feasibility study. *J Ultrasound Med* 2008; **27**: 935-946 [PMID: 18499853]

7 **Inoue T**, Kudo M, Hatanaka K, Arizumi T, Takita M, Kitai S, Yada N, Hagiwara S, Minami Y, Sakurai T, Ueshima K, Nishida N. Usefulness of contrast-enhanced ultrasonography to evaluate the post-treatment responses of radiofrequency ablation for hepatocellular carcinoma: comparison with dynamic CT. *Oncology* 2013; **84** Suppl 1: 51-57 [PMID: 23428859 DOI: 10.1159/000345890]

8 **Morimoto M**, Sugimori K, Shirato K, Kokawa A, Tomita N, Saito T, Tanaka N, Nozawa A, Hara M, Sekihara H, Shimada H, Imada T, Tanaka K. Treatment of hepatocellular carcinoma with radiofrequency ablation: radiologic-histologic correlation during follow-up periods. *Hepatology* 2002; **35**: 1467-1475 [PMID: 12029632]

9 **Koda M**, Tokunaga S, Miyoshi K, Kishina M, Fujise Y, Kato J, Matono T, Okamoto K, Murawaki Y, Kakite S. Assessment of ablative margin by unenhanced magnetic resonance imaging after radiofrequency ablation for hepatocellular carcinoma. *Eur J Radiol* 2012; **81**: 2730-2736 [PMID: 22137612 DOI: 10.1016/j.ejrad.2011.11.013]

10 **Faroja M**, Ahmed M, Appelbaum L, Ben-David E, Moussa M, Sosna J, Nissenbaum I, Goldberg SN. Irreversible electroporation ablation: is all the damage nonthermal? *Radiology* 2013; **266**: 462-470 [PMID: 23169795 DOI: 10.1148/radiol.12120609]

P- Reviewer: Rossi RE, Ruzzenente A **S- Editor**: Ma YJ
L- Editor: A **E- Editor**: Wang CH

Accepted Article

Basic FGF-treated adipose tissue-derived mesenchymal stem cell infusion ameliorate liver cirrhosis via paracrine HGF

Wei-Ping Tang[1], Tomohiko Akahoshi[1,2], Jing-Shu Piao[1], Sayoko Narahara[1], Masaharu Murata[1], Takahito Kawano[1], Nobuhito Hamano[1], Ikeda Tetsuo[2], Makoto Hashizume[1]

[1] Department of Disaster and Emergency Medicine, Faculty of Medicine, Kyushu University, Fukuoka, Japan

[2] Department of Surgery and Science, Graduate School of Medical Sciences, Kyushu University, Fukuoka, Japan

Correspondence to:

Tomohiko Akahoshi

Department of Disaster and Emergency Medicine, Faculty of Medicine, Kyushu University, 3-1-1 Maidashi, Higashi-ku, Fukuoka 812-8582, Japan

E-mail: tomohiko@surg2.med.kyushu-u.ac.jp

This article has been accepted for publication and undergone full peer review but has not been through the copyediting, typesetting, pagination and proofreading process, which may lead to differences between this version and the Version of Record. Please cite this article as doi: 10.1111/jgh.12893

This article is protected by copyright. All rights reserved.

Tel: 81-92-642-6223; Fax: 81-92-642-6224

Running title:

ADSCs relieve liver cirrhosis via HGF

Abbreviations

ADSCs, adipose tissue-derived mesenchymal stem cells

bFGF, basic fibroblast growth factor

HSCs, hepatic stellate cells

HGF, hepatocyte growth factor

CCl_4, carbon tetrachloride

PBS, phosphate-buffered saline

HNF4a, hepatocyte nuclear factor 4 alpha

This article is protected by copyright. All rights reserved.

Accepted Article

Accepted Article

Abstract

Background and Aim: Recent studies show that adipose tissue-derived mesenchymal stem cells have potential clinical applications. However, the mechanism has not been fully elucidated yet. Here, we investigated the effect of basic fibroblast growth factor-treated adipose tissue-derived mesenchymal stem cells infusion on a liver fibrosis rat model and elucidated the underlying mechanism.

Methods: Adipose tissue-derived mesenchymal stem cells were infused into carbon tetrachloride-induced hepatic fibrosis rats through caudal vein. Liver functions and pathological changes were assessed. A co-culture model was used to clarify the potential mechanism.

Results: basic fibroblast growth factor treatment markedly improved the proliferation, differentiation and hepatocyte growth factor expression ability of adipose tissue-derived mesenchymal stem cells. Although adipose tissue-derived mesenchymal stem cells infusion alone slightly ameliorated liver functions and suppressed fibrosis progression, basic fibroblast growth factor-treatment significantly enhanced the therapeutic effect in association with elevated hepatocyte growth factor expression. Moreover,

This article is protected by copyright. All rights reserved.

Accepted Article

double-immunofluorescence staining confirmed that the infused cells located in fibrosis area. Furthermore, co-culture with adipose tissue-derived mesenchymal stem cell led to induction of hepatic stellate cell apoptosis and enhanced hepatocyte proliferation. However, these effects were significantly weakened by knockdown of hepatocyte growth factor. Mechanism investigation revealed that co-culture with adipose tissue-derived mesenchymal stem cells activated JNK-p53 signaling in hepatic stellate cell and promoted apoptosis.

Conclusions: basic fibroblast growth factor treatment enhanced the therapeutic effect of adipose tissue-derived mesenchymal stem cells, and secretion of hepatocyte growth factor from adipose tissue-derived mesenchymal stem cells plays a critical role in amelioration of liver injury and regression of fibrosis.

Keywords:

ADSCs, bFGF, liver cirrhosis, HGF, RNA interference

This article is protected by copyright. All rights reserved.

Accepted Article

Introduction

Liver cirrhosis is characterized by parenchymal fibrosis associated with liver dysfunction [1–3]. There is no effective therapy apart from liver transplantation. Recent stem cell therapies have progressed significantly [4-6]. Of these approaches, bone marrow cells have been reported as an effective therapeutic agent for hepatitis patients [7,8]. However, it is difficult to obtain bone marrow cells because of painful procedures and relatively low cell yields [9]. Therefore, a cell source with an easier approach for isolation is desirable for cell therapy. Adipose tissue-derived mesenchymal stem cells (ADSCs) are an attractive cell source for regenerative medicine because of their multipotency [10,11]. ADSCs can differentiate into multiple lineages such as hepatocytes and blood vessels [12,13]. Compared with bone marrow cells, ADSCs can be easily obtained in large numbers by minimally invasive methods, and show better immunocompatibility [14]. Moreover, there are increasing studies of the ability of ADSCs to mediate anti-inflammatory and healing effects via paracrine cytokines such as hepatocyte growth factor (HGF) and vascular endothelial growth factor [15,16]. However, the underlying mechanism of the antifibrotic effect of ADSCs is largely unknown.

This article is protected by copyright. All rights reserved.

Accepted Article

In the present study, we hypothesized that bFGF-treated ADSC infusion may enhance the amelioration of liver fibrogenesis and the recovery of liver dysfunction in a CCl_4-induced cirrhosis rat model via overexpressing HGF. To test this hypothesis, we infused ADSCs into hepatic cirrhosis rats, and confirmed their homing by bio-fluorescence imaging and double-immunofluorescence staining. Furthermore, a co-culture model was employed to investigate the influence of ADSCs on hepatic stellate cells (HSCs) and hepatocytes, and elucidate the underlying mechanism. Moreover, to identify the role of HGF, we transfected ADSCs with HGF siRNA followed by co-culture with HSCs or hepatocytes.

Methods

ADSC preparation and characteristics

Six-week-old male Fischer 344 rats (Charles River, Atsugi, Japan) were housed under controlled temperature, humidity, and lighting conditions. The study was approved by the Committee of Animal Experiment Ethics at Kyushu University. All procedures were carried out in strict accordance with the approved experimental plan.

Rat ADSCs were collected from the inguinal fat pad [17]. Briefly, adipose tissues were minced, digested in 1 mg/mL collagenase (Sigma-Aldrich, St. Louis, Germany),

This article is protected by copyright. All rights reserved.